that the branch unbalance Q is related to a relaxation of the stimulated quasiparticle current $j_{qp}(\omega)$ to the supercurrent state as at a single S/N boundary. In the stimulated link, both the quasiparticle current and supercurrent oscillate. Thus a maximum interaction would be expected when the time average of $\vec{j}_s \cdot \vec{j}_{qp}$ is also at a maximum. This will occur at power levels which maximize this product.

At finite voltage $V_{S_1S_2}$, current "steps" in the presence of rf showed a similar phenomenon. The usual current steps with zero dynamic resistance on the $V_{S_1S_2}$-I curve of the bridge were replaced by a region of current-dependent negative and positive dynamic resistance on curve V_{S_1W} and its complementary characteristic V_{WS_2} across the other SW boundary (see Fig. 2). Their sum, however, gives back the normal constant-voltage steps for the entire bridge at the correct Josephson voltages. These measurements also indicate that an extra potential is stimulated within the link by the external radiation and that this potential changes sign as the bias current is increased through the step. The sign of the extra potential is also a function of rf power, similar to the effect at zero voltage.

We also note that the existence of such nonequilibrium quasiparticle currents in the link could also be related to the "excess current" often observed in conducting weak links. The existence of the link potential also implies that no simple model of a conducting link composed of a Josephson current and passive circuit elements can completely describe the oscillating link.

*Work supported in part by the U. S. Office of Naval Research under Contract No. N00014-A-0094-0013, and by the U. S. Energy Research and Development Administration.

[1]T. J. Rieger, D. J. Scalapino, and J. E. Mercereau, Phys. Rev. B 6, 1734 (1972).

[2]W. J. Skocpol, M. R. Beasley, and M. Tinkham, J. Low Temp. Phys. 16, 145 (1974).

[3]H. A. Notarys and J. E. Mercereau, J. Appl. Phys. 44, 1821 (1973).

[4]D. W. Palmer and S. K. Decker, Rev. Sci. Instrum. 44, 1621 (1973).

[5]R. K. Kirschman and J. E. Mercereau, Phys. Lett. 35A, 177 (1971).

[6]J. Clarke, Phys. Rev. Lett. 28, 1363 (1972).

[7]M. L. Yu and J. E. Mercereau, Phys. Rev. B 12, 4909 (1975).

[8]Detail comparison is not possible at the present moment. But we can have an order-of-magnitude estimate. The bridge with which results on Figs. 1 and 2 were obtained in 38 μm wide, 1 μm long, and 150 Å thick. If we use Eq. (14) in Ref. 7 with $\tau_Q \cong 10^{-10}$ sec, $N(0) \cong 10^{23}$/eV cm^3, and $\langle \nabla \cdot \vec{j}_s \rangle \cong j_c/L$, is the length of the bridge, $\langle \mu_p - \mu \rangle$ is about 10^{-7} eV which is in reasonable agreement with the experiment.

Dynamic Polarization Echoes in Powders

K. Kajimura,* K. Fossheim,† T. G. Kazyaka, R. L. Melcher, and N. S. Shiren
IBM Thomas J. Watson Research Center, Yorktown Heights, New York 10598
(Received 9 August 1976)

Piezoelectric powders excited by two or more rf pulses are found to exhibit echoes characteristic of anharmonic oscillators. At high rf powers, the echoes show complex dependence upon the pulse separation, power, and widths.

Powder samples are observed to radiate coherently two-pulse (e_2) and three-pulse (e_3) echoes at times $t = m\tau$ and $t = nT \pm p\tau$ ($m = 2, 3, 4, \ldots$; $n = 1, 2, 3, \ldots$; $p = 1, 2, 3, \ldots$) when electromagnetic pulses are applied at times $t = 0$, τ, and T.[1-5] The decay of e_2 with τ, and of e_3 with T, are described by the decay constants T_2 and T_1, respectively. In those cases in which T_1 is short enough to be associated with some dynamic behavior of the particles of the powder, the echo phenomena are termed "dynamic." Under other conditions, when T_1 is long (often exceeding days), the echo phenomena are properly termed "static" or "storage" echoes. As described previously,[6] the storage-echo formation process involves the physical reorientation of the individual particles of the powder.

The purpose of this Letter is to describe new experimental results on the dynamic echo process in powders. These results clearly demonstrate that the dominant mechanism for echo formation is an anharmonicity in the mechanical oscillation of the particles which couples the oscillations started by the applied pulses and is effective during the time following the pulses. This anharmonic-oscillator model is to be distinguished

from field-mode interaction mechanisms in which the electromagnetic field of the second pulse interacts with the modes excited by the first pulse. The characteristic feature of the anharmonic-oscillator model is a "build up" period during which the echo amplitude, e_2, increases with increasing pulse separation, τ, from $e_2 = 0$ at $\tau = 0$.[7] In contrast, echoes derived from field-mode interactions (e.g., storage echoes in powders,[6] polarization echoes in single crystals, or spin echoes) are maximum for $\tau = 0$ and generally decrease monotonically with increasing τ. We also report here on the observation of several new high-power echo phenomena in which are found complicated but consistent dependences of the echo amplitude and shape on τ and the applied-pulse area (where the area, A, is the product of the amplitude, E, and the width, Δ, of the pulse).

In the descriptions of previous experimental work on polarization echoes in magnetoelastic,[1] metallic,[2] and piezoelectric[3-5] powders, no attempt was made to distinguish between anharmonic-oscillator mechanisms and field-mode interactions. The distinguishing features of anharmonic-oscillator models were dealt with extensively by Gould,[8] and by Herrman, Kaplan, and Hill[9] in their work on plasma and ferrimagnetic echoes. However, in previous theoretical work on polarization echoes, either the *de facto* assumption was made that field-mode interactions dominate[10,11] or the fundamental characteristic of the anharmonic-oscillator model as described above was not recognized.[3,5]

In the experimental work on piezoelectric powders described in this Letter, the samples were all sealed in vacuum, except in one case stated below. Storage-echo phenomena[6] were suppressed to at least 20 dB below the dynamic phenomena of interest here, either through the use of low-amplitude pulses at microwave frequencies (X and Ku band), or through the deliberate introduction of phase incoherence between applied VHF pulses (15–300 MHz). The receiver dead time after an applied pulse was 4–6 μsec at VHF and 20 nsec at X and Ku band. At VHF, a typical sample consisted of approximately 10^6 particles, whose diameters ranged from 50 to 60 μm, placed between capacitor plates separated by 1 mm. At microwave frequencies, the samples consisted of 10^{13} submicron particles contained in a glass capsule placed in a wave guide. Unless otherwise specified, only the two-pulse echo, e_2, occurring at $t = 2\tau$ will be discussed below, although the higher-order dynamic echoes mentioned above were also observed.

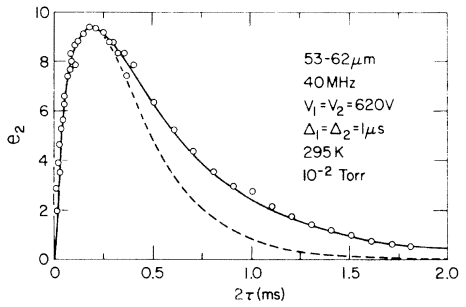

FIG. 1. Two pulse echo amplitude, e_2, on a linear scale versus pulse separation, τ, in GaAs at room temperature. Dashed curve is Eq. (2) with $T_2 = 270$ μsec. Solid curve is obtained from Eq. (2) summed over a Maxwellian distribution in $\Gamma - \Gamma_c$ ($\Gamma_c = 400$ sec^{-1}).

In Fig. 1, we show the dependence of the two-pulse echo amplitude, e_2, on the pulse separation, τ, in high-resistivity GaAs powder. The data show very clearly that e_2 goes to zero for $\tau = 0$ and decays exponentially for $\tau \to \infty$. These data definitively show that the nonlinear interaction responsible for echo formation occurs during the time interval *after* the second pulse is applied, as expected for the anharmonic-oscillator model. Any field-mode interaction occurs only *during* the second pulse and is, therefore, maximum for $\tau = 0$. Ferrimagnetic echoes in yttrium-iron-garnet single crystals and plasma echoes[12] are the only previous examples of "build up" behavior similar to that shown in Fig. 1. Using low-amplitude pulses in quartz and $LiNbO_3$ at VHF and in ZnO at microwave frequencies, the decay behavior of e_2 is qualitatively similar to that shown in Fig. 1. In materials with short T_2, the failure to observe the build-up at small τ can be attributed to the receiver dead time. This effect was demonstrated in GaAs by increasing T_2 from values of 4–8 μsec to as large as 600 μsec by removing surface damage from the particles through etching.

Models of anharmonic oscillators can be classified according to whether they lead to nonlinear dispersion, absorption, or to both dispersion and absorption. The nonlinear absorption can either increase with amplitude (as in harmonic generation) or decrease with amplitude (as in the coupling to a saturable resonance or relaxation absorber). Although it is not the purpose of this Letter to discuss theoretical models in detail, we note that at low power all anharmonic-oscillator models are indistinguishable. As a representative model, we consider here a single mode of

oscillation for each particle and take the nonlinear dispersion resulting from the fourth-order lattice anharmonicity. The wave equation for the elastic displacement, $u(x, t)$, corresponding to this mode of a particle may be written

$$\ddot{u} + 2\Gamma\dot{u} - (c_2/\rho)u_{xx} - (c_4/2\rho)u_x^2 u_{xx} = 0, \quad (1)$$

where $\Gamma = 1/T_2$, ρ is the mass density, c_2 and c_4 are, respectively, the effective second- and fourth-order elastic constants, and subscripts denote space derivatives. For given initial conditions, Eq. (1) can be solved analytically for the time evolution of the amplitude and phase in the slowly-varying-envelope approximation. The appropriate initial conditions are given by the mode amplitudes at times $t = 0$ and τ as determined by the piezoelectric excitation of the particle by the applied pulse. Summing the solutions to Eq. (1) over the distribution of natural particle frequencies, the coherent response of the sample at $t = 2\tau$ and for small applied-pulse areas A_1 and A_2 can be written

$$e_2 = \gamma T_2 A_1 A_2^2 [1 - \exp(-2\tau/T_2)] \times \exp(-2\tau/T_2), \quad (2)$$

where γ is proportional to c_4/c_2. For $2\tau \ll T_2$, we have $e_2 \propto \tau$, in agreement with a similar model described in Refs. 8 and 9. By proper inclusion of the linear decay rate $\Gamma(=1/T_2)$, we are able to derive the expected decay behavior for all τ. This result [Eq. (2)] is in qualitative but not quantitative agreement with experiment as shown by the dashed curve in Fig. 1. If, as is quite reasonable, we assume that there is a distribution of Γ's in the sample and sum Eq. (2) over the distribution, the solid curve is obtained in good agreement with the data. A similarly good fit to the data is obtained by choosing as few as two different Γ's.

The higher-order echoes at $t = 3\tau$, 4τ, 5τ, ... which are observed experimentally follow directly from the anharmonic-oscillator model. It is not necessary to assume, as has been suggested,[10] that the echoes themselves act as pulses in generating subsequent echoes. For large τ ($2\Gamma\tau \gg 1$) the decay of the $m\tau$ two-pulse echo is given theoretically as $\exp[-2(m-1)\tau/T_2]$; this is in agreement with experiment in GaAs.

We find that the value of γ [Eq. (2)] varies less than a factor of 2 over the temperature range 4.2 K $< T <$ 400 K in GaAs, $LiNbO_3$, and quartz at VHF. This is quite different from the temperature dependence reported in Ref. 5.

Measurements of T_2 at VHF with the powder immersed in gases of different acoustic impedances are in quantitative agreement with the acoustic-impedance-mismatch model of energy transfer from solid to gas. This is also in agreement with the observed linear frequency dependence of Γ in the gas. In high vacuum, we find $\Gamma \propto \omega^2$ at room temperature.

At the highest VHF powers attainable in our experiments (corresponding to applied voltages of 10^3 V across a 1-mm sample), the decay behavior in GaAs becomes weakly power dependent. This is not unexpected since Eq. (2) is valid only at low power. However, at liquid-helium temperature in quartz at VHF and in ZnO at microwave frequencies, the decay behavior becomes extremely power sensitive even at moderate powers (voltages of 200 V at VHF and 2 V at X band) and qualitatively different from that shown in Fig. 1. Typical data for quartz are shown in Fig. 2. Note that the echo shape is extremely sensitive to τ and changes from a triangular shape with a base width of 2Δ (where Δ is the applied pulse width) at small τ to a rectangular shape with width Δ at large τ. The amplitude of the center of the echo is given by the data points on the curve. The very pronounced dip for $\tau_{dip} \simeq 185$ μsec is observed only when $A_1 \gtrsim A_2$, and then only for large A_1 and A_2. When $A_2 > A_1$ and both are large, the

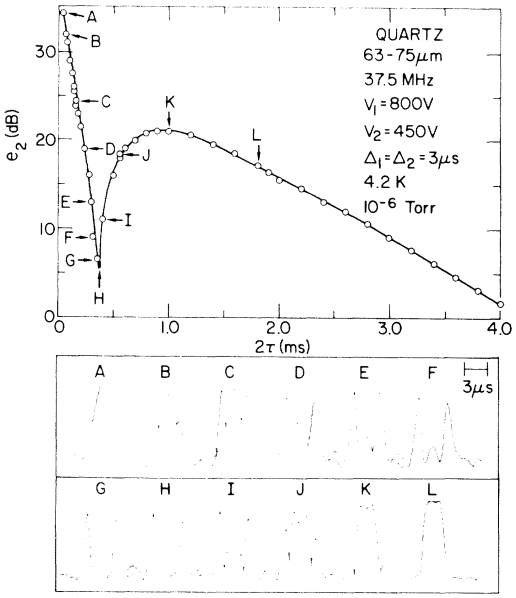

FIG. 2. The bottom panel shows the shapes of echoes at different τ as indicated on the curve in the upper panel which shows the amplitude at the center of the echo as a function of 2τ.

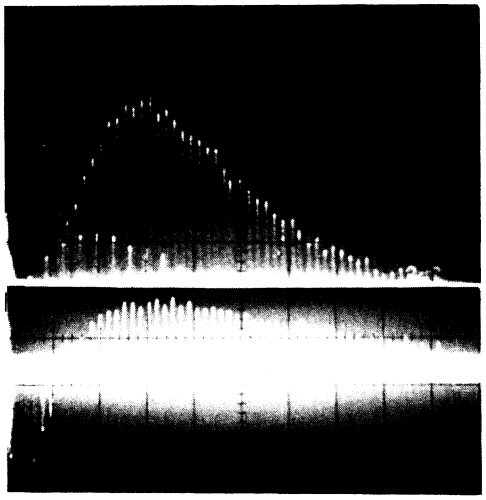

FIG. 3. e_2 versus τ in ZnO at 1.25 K and 9.0 GHz for A_1 6 dB higher than A_2, 100-nsec pulses; horizontal scale 2 μsec/cm. Top trace: amplitude detection (3τ echoes are also visible). Bottom trace: phase sensitive detection.

echo decays monotonically from a maximum at $\tau = 0$. Thus, the high-power behavior contrasts with the simple expression, $A_1 A_2^2$, expected at low powers [Eq. (2)]. For small A_1 and A_2, the decay behavior is similar to that shown in Fig. 1, independent of the ratio of A_1 to A_2, and the echo shapes are independent of τ. In ZnO at X and *Ku* band, the decay behavior is similar to that in quartz at VHF. However, in the region of the dip, the echo shapes for ZnO exhibit less pronounced structure than indicated in Fig. 2. The X-band data also show that whenever a dip appears in the e_2 vs τ curve, the echo phase for $\tau < \tau_{\text{dip}}$ differs from that of $\tau > \tau_{\text{dip}}$ by approximately π, as shown in Fig. 3.

There is little doubt that the complicated decay and echo shape behavior indicated above is a consequence of the use of high-amplitude and/or finite-width pulses. Evaluation of the nonlinear dispersion model described by Eq. (1) for finite-width pulses indeed shows τ-dependent echo shapes and decay behavior somewhat similar to those shown in Fig. 2 and discussed above. However, quantitative agreement has so far not been achieved. Calculations based on a nonlinear relaxation absorber using δ-function pulses are in quite good agreement with the observed decay behavior. Echo shapes cannot, of course, be extracted from a theory based upon δ-function pulses. The transition from low-power to high-power behavior depends not only on the applied pulse areas, but also on the magnitude of the nonlinear coupling constant, the piezoelectric coefficient, and the damping constant of the particles.

We note that the data shown in Fig. 2 do not exclude the possibility of a field-mode interaction dominating at small τ, since there is no indication that $e_2 \to 0$ at $\tau = 0$. Since the nonlinear dispersion, as well as the relaxation-absorption models, predict an extremely short build-up region at high power when $A_1 > A_2$, it may be that the build-up was obscured by the receiver dead-time. Note that the data of Fig. 3 do show a build-up region.

The behavior shown in Fig. 2 is sensitive to temperature. At VHF in quartz at room temperature, the structure in the decay curve and the echo shapes is much less pronounced than that shown in Fig. 2. In ZnO at X and *Ku* band, small changes in the temperature in the liquid-helium range cause significant changes in the structure of the curve. These temperature effects at high power may be attributable to the temperature dependence of the effective nonlinearity, γT_2 [Eq. (1)]. Alternatively, if the relaxation-absorber model is used, the temperature dependence of the relaxation rate of $1/\tau_d$ of the absorber could cause the observed effects.

In conclusion, we remark that although the work reported here was restricted to piezoelectric particles, it is reasonable to believe that anharmonic-oscillator mechanisms are also responsible for dynamic echoes in magnetoelastic and metallic powders. The various anharmonic-oscillator models are distinguishable only in high-power experiments; therefore, experimental work of the type reported here should facilitate determination of the precise mechanism in each case.

The technical contributions of D. R. Vigliotti to this work are gratefully acknowledged. One of the authors (K.F.) would like to acknowledge the partial support of the Norwegian Research Council for Science and the Humanities.

*Permanent address: Electrotechnical Laboratory, Tanashi, Tokyo, Japan.

†Permanent address: Department of Physics, The Norwegian Institute of Technology, 7034 Trondheim, Norway.

[1]M. Rubinstein and G. H. Stauss, J. Appl. Phys. 39, 81 (1968).

[2]S. Kupca and C. W. Searle, Can. J. Phys. 53, 2622 (1975), and references contained therein.

[3]G. A. Smolenskii, N. N. Krainik, S. N. Popov, and B. D. Laikhtman, in Proceedings of the Third European

Meeting on Ferroelectricity, Zurich, Switzerland, 22-26 September 1975 (to be published).
[4]V. M. Berezov, Ya. Ya. Asadullin, and V. D. Korepanov, Zh. Eksp. Teor. Fiz. 69, 1674 (1975) [Sov. Phys. JETP (to be published)].
[5]P. I. Kuindersma, S. Huizenga, J. Kommandeur, and G. A. Sawatzky, Phys. Rev. B 13, 496 (1976).
[6]R. L. Melcher and N. S. Shiren, Phys. Rev. Lett. 36, 888 (1976).
[7]K. Kajimura, K. Fossheim, R. L. Melcher, and N. S. Shiren, Bull. Am. Phys. Soc. 21, 293 (1976).
[8]R. W. Gould, Phys. Lett. 19, 477 (1965).
[9]G. F. Herrmann, D. E. Kaplan, and R. M. Hill, Phys. Rev. 181, 829 (1969).
[10]B. D. Laikhtman, Fiz. Tverd. Tela 17, 3278 (1975) [Sov. Phys. Solid State 17, 2154 (1976)].
[11]N. N. Krainik, V. V. Lemanov, S. N. Popov, and G. A. Smolenskii, Fiz. Tverd. Tela 17, 2462 (1975) [Sov. Phys. Solid State 17, 1635 (1976)].
[12]D. E. Kaplan, R. M. Hill, and G. F. Herrmann, J. Appl. Phys. 40, 1164 (1969); G. F. Herrmann, R. M. Hill, and D. E. Kaplan, Phys. Rev. 156, 118 (1967).

Origin of Raman Scattering and Ferroelectricity in Oxidic Perovskites

R. Migoni and H. Bilz
Max-Planck-Institut für Festkörperforschung, 7000 Stuttgart-80, West Germany

and

D. Bäuerle
Fachbereich Physik der Universität Osnabrück, 4500 Osnabrück, West Germany
(Received 9 July 1976)

The second-order Raman scattering and the temperature dependence of the ferroelectric soft mode in ABO_3 perovskites are explained quantitatively in terms of a nonlinear shell model by assuming an anisotropy in the oxygen polarizability. This model yields a new explanation for the origin of ferroelectricity in perovskites.

In 1960 Cochran and Anderson[1] developed the soft mode concept, which explains the ferroelectric phase transition in a great variety of ionic crystals. In this theory a compensation of long- and short-range forces leads to a strongly anharmonic behavior of the ferroelectric soft mode, $\omega_F \equiv \omega_{T_1 0}(\Gamma)$, whose temperature dependence is approximately described by

$$\omega_F^2 = A(T - T_c). \quad (1)$$

In the last fifteen years, many experimental and theoretical studies have been carried out in order to further clarify the details of the soft mode behavior,[2] particularly in the ABO_3 perovskites. The explanation of the temperature dependence of the soft mode in terms of anharmonic interactions has been discussed[3-7] and quantitative results have been obtained using an effective quartic potential between the central B ion and its neighboring O ions.[4,5,7] In order to describe the temperature dependence of ω_F, however, an unrealistic fourth-order parameter had to be used.[4,7]

In this Letter we show that in ABO_3 perovskites the behavior of the ferroelectric soft mode and related properties may be explained by the strongly anisotropic deformability of the oxygen ion, which also determines the second-order Raman scattering in these crystals.

The following facts led us to focus our attention on the polarizability of the oxygen ion: (a) The only perovskites which are known to show ferroelectric soft modes are the oxidic ones; (b) these are also the only ones which show a strong second-order Raman effect; (c) in simple cubic oxides (such as MgO, etc.), the Raman scattering is dominated by the *intra*-ionic polarizability of the oxygen ion[8-10]; and (d) it is known that the oxygen polarizability depends strongly on its environment in a crystal.[11-13]

In order to account for the intra-ionic anisotropy of the oxygen polarizability $\alpha(O^{--})$, we modify the shell model of Cowley[14] and Stirling[15] by replacing the core-shell force constant by a tensor with two parameters, K_{OA} and K_{OB} (cf. Table I). We denote the corresponding components of the tensor $\alpha(O^{--})$ in the directions of neighboring A and B ions by α_{OA} and α_{OB}, respectively. Calculations have been performed for $SrTiO_3$ and $KTaO_3$. Both crystals are cubic and show a ferroelectric soft mode, but they differ strongly in the ionic masses and charges. In the case of $KTaO_3$, only the lower phonon branches have been measured by neutron spectroscopy,[16] and the results are therefore less reliable. In order to calculate the second-order Raman spectra, we use a nonlinear extension of $\alpha(O^{--})$.

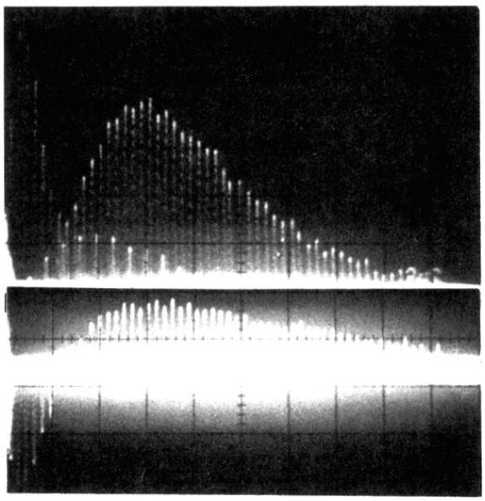

FIG. 3. e_2 versus τ in ZnO at 1.25 K and 9.0 GHz for A_1 6 dB higher than A_2, 100-nsec pulses; horizontal scale 2 μsec/cm. Top trace: amplitude detection (3τ echoes are also visible). Bottom trace: phase sensitive detection.